DISPEC TRAINING SCHOOL

Ground-based and spaceborne monitoring systems and their data processing techniques

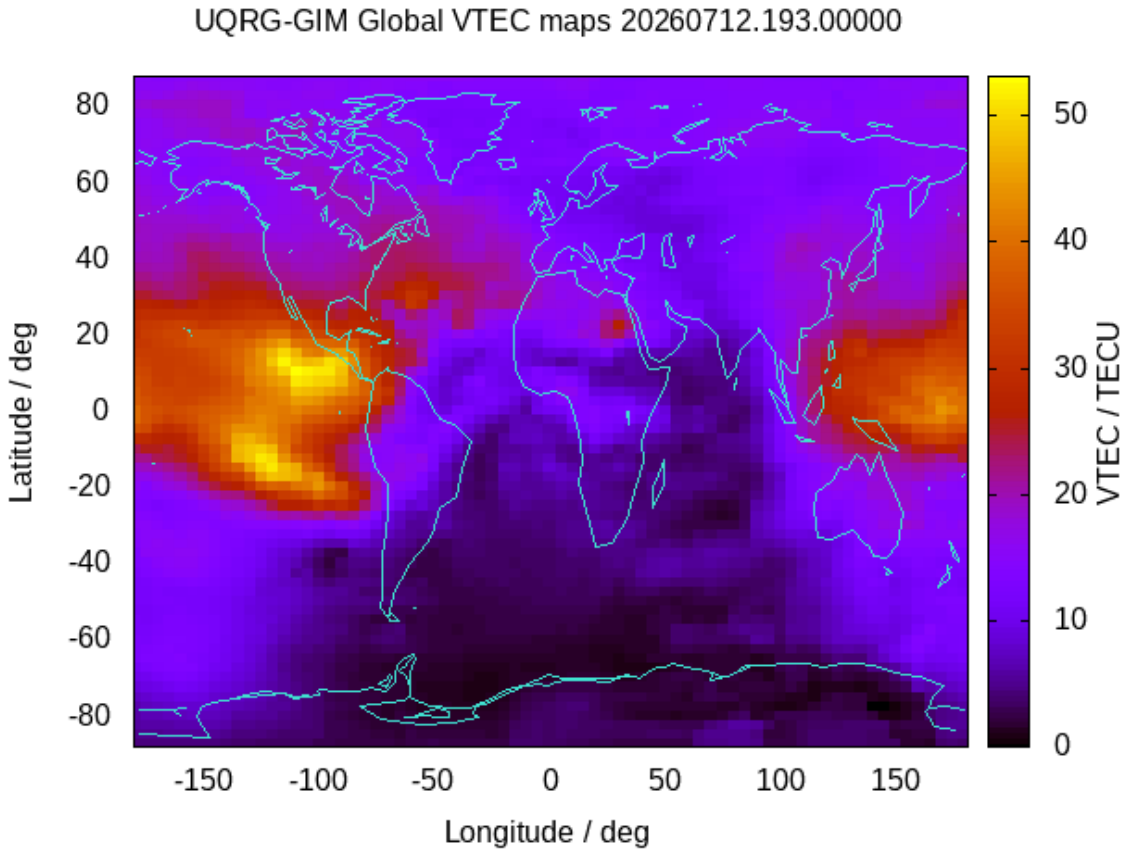

Ivan Galkin (1) and Manuel Hernandez-Pajares (2)
(1) University of Massachusetts Lowell,USA
(2) UPC-IonSAT Research Group, IGS Associate Analysis Center, Spain

3.2.1 A spaceborne ionospheric tomography *blackboard*

- Global navigation satellite system (GNSS) radio-occultation (RO) missions, such as GPS/MET (Hernández-Pajares et al. 1990), CHAMP (Jakowski et al. 2002), COSMIC/ FORMOSAT-3 (Olivares-Pulido et al. 2016), GRACE, PAZ (Cardellach et al. 2019), FY3C/GNOS RO (Mao et al. 2016), and the EPS-SG mission recently launched (see previous study in Hernández-Pajares et al. 2017), are of great benefit to ionospheric sounding and modeling.

- The ground based ionospheric measurements, like those from GNSS transmitters, present a typical line-of-sight vertical geometry that provides an associated high horizontal resolution and poor vertical one, suitable nevertheless for an accurate global ionospheric electron content estimation (e.g. Hernández-Pajares et al. 1999, and figures 1a, 1b & 1c, where it is shown that considering low vertical resolution variability significantly helps).

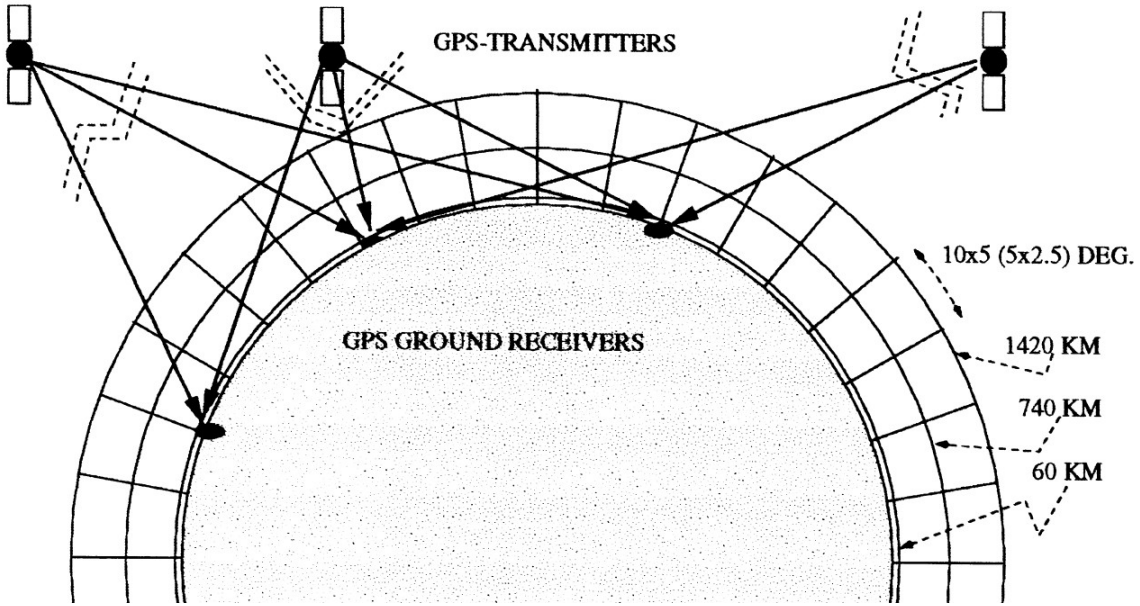

Figure 1a. 2D layout of the 3D voxel-based model of electron content distribution based on multifrequency GNSS signals gathered from a global network of ground-based receivers (from Hernández-Pajares et al. 1999).

Ionospheric tomography reduces the error in the calculation of global ionosphere maps (GIM) of VTEC at all latitudes.

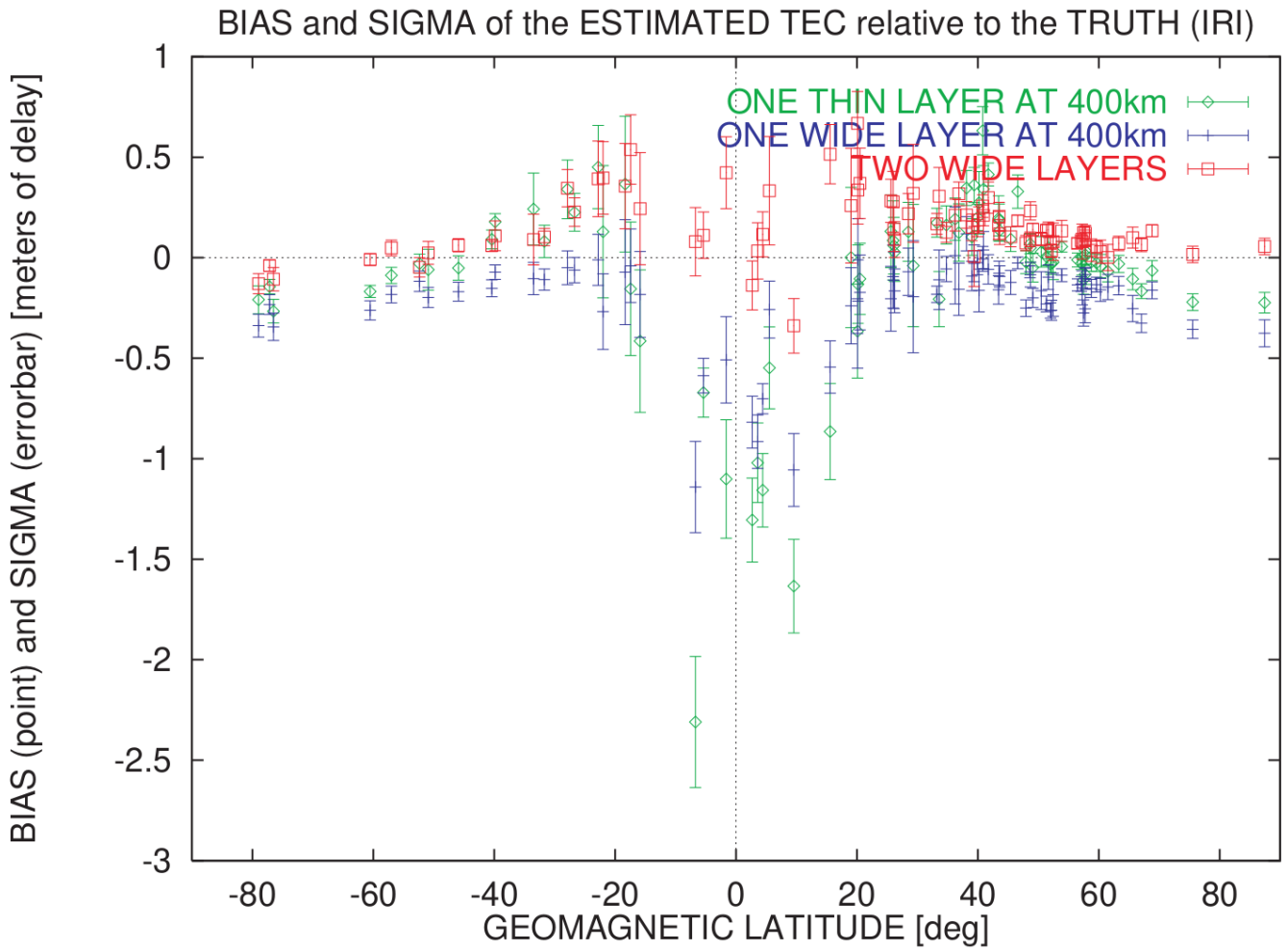

Figure 1b. Typical reduction of the error when a dual-shell model is used for VTEC estimation in front of the widely used single layer model (extracted from Hernández-Pajares et al. 1999).

Ionospheric tomography reduces the error in the calculation of global ionosphere maps (GIM) of VTEC at all latitudes.

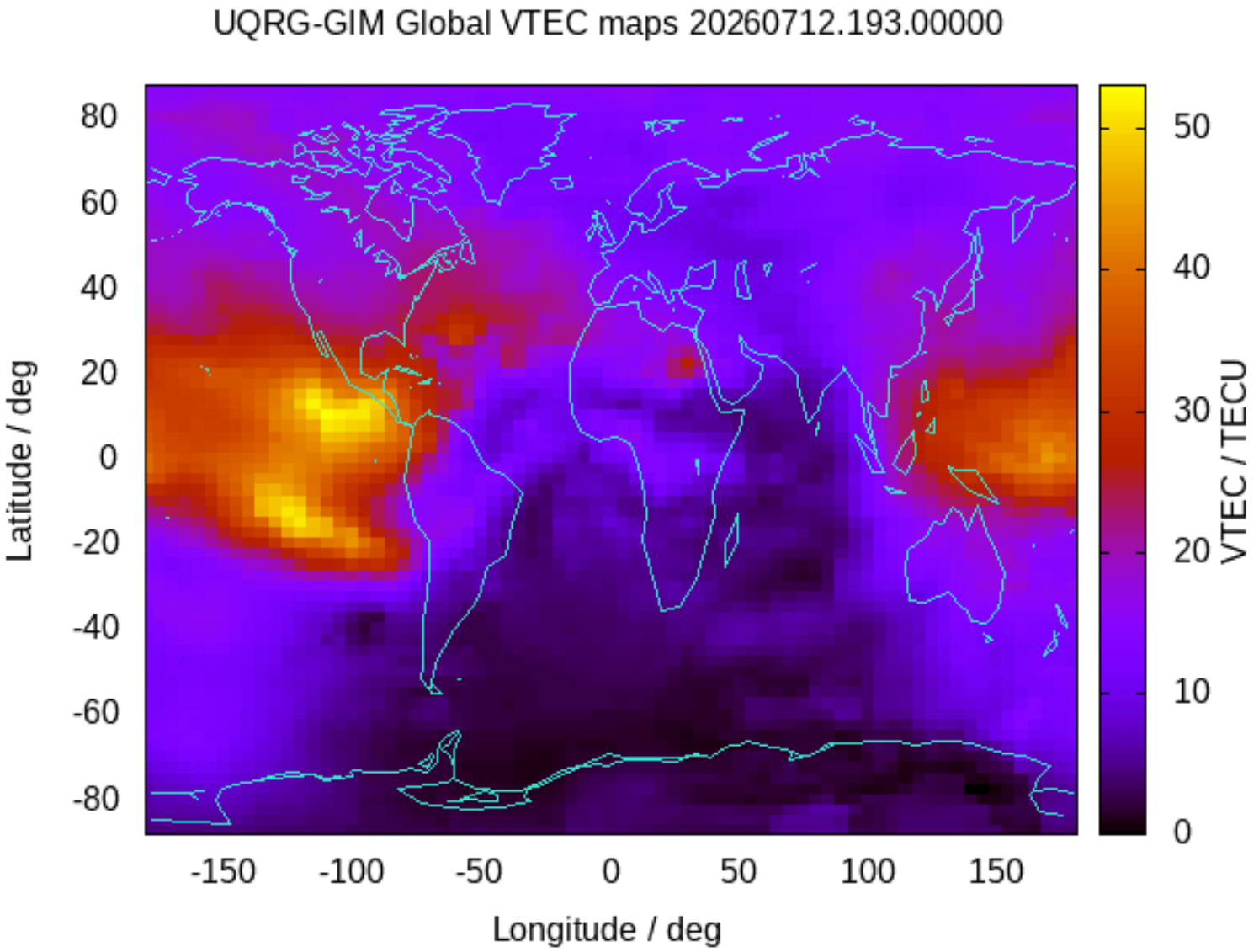

Figure 1c. Animation of rapid "UQRG" VTEC Global Ionospheric Maps, computed from +200 ground GNSS receeivers with the two-shell (AKA dual layer) voxel model solved in a Kalman filter by UPC-IonSAT with TOMION, and for the International GNSS Service, IGS (day 193 of year 2026, the most recent available when these notes were written, see details for instance in Roma-Dollase et al. 2018 and in Hernández-Pajares et al. 2009).

Ionospheric tomography from almost vertical scans of the ionosphere given by the GNSS radio-occultations measurements

Let's summarize some of the challenges of the associated tomographic problem:

-The Low Earth Orbiting ionospheric measurements of GNSS transmitters, in radio-occultation scenario (i.e. below the local horizon) provides a vertical scanning with an associated very high vertical resolution (but with a limited horizontal one).

- This can be seen, e.g. in Hernández-Pajares et al. 2000, and in figures 2 & 3a, and Table 2: layout and validation with observations of the GPS/MET mission and with International Reference Ionosphere, IRI, for validation.

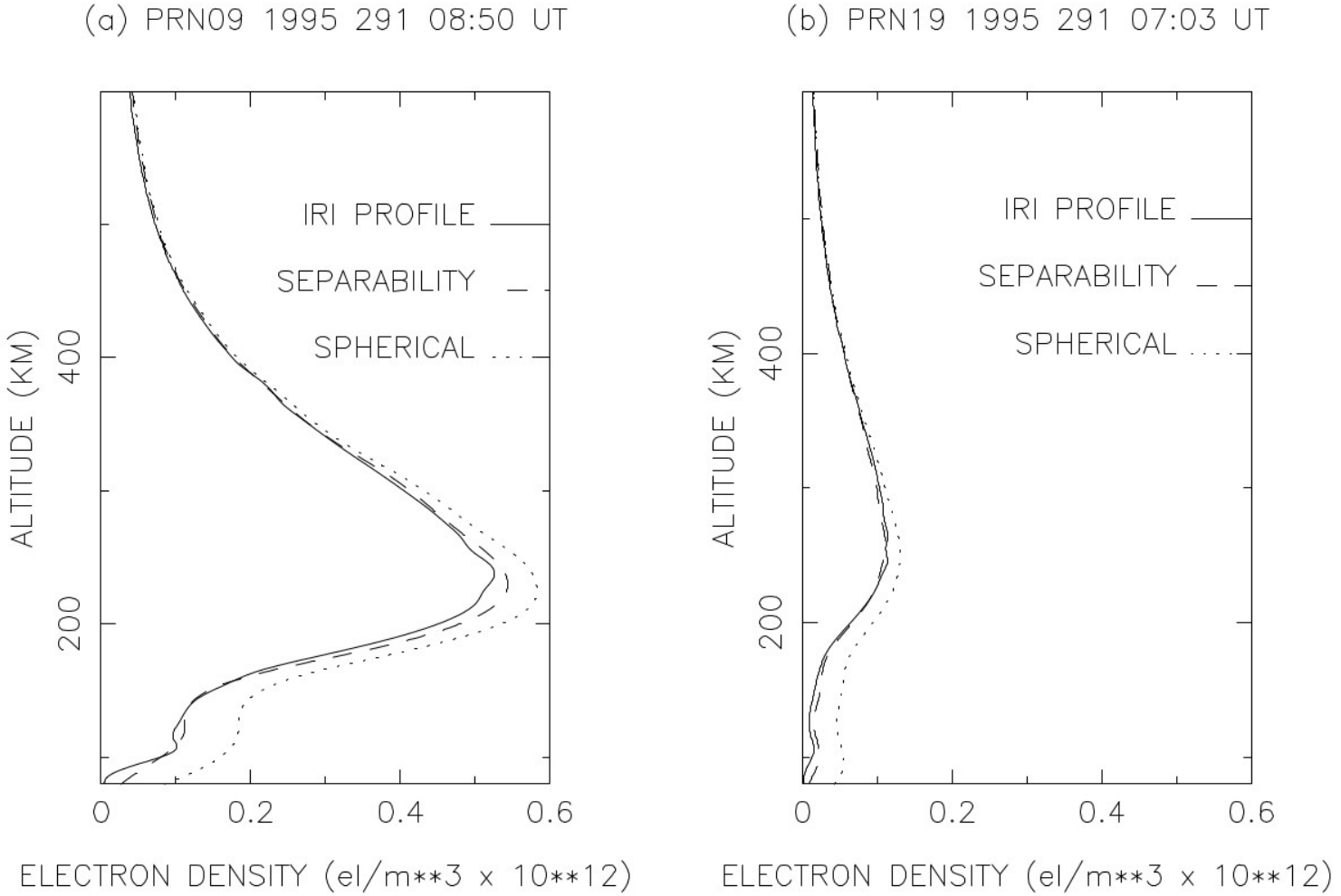

Figure 2. Example of performance of the traditional (spherical symmetry assumption) vs the improved (separability) Abel inversion algorithms for two radio-occultations of the first of these missions (GPS/MET) but using IRI simulated slant ionospheric delays, and correspondingly IRI electron density as ground truth (extracted from Hernández-Pajares et al. 2000).

Validation vs ionosonde data & new challenging GNSS radio-occultation scenarios

	Internal comparisons		foF2 all LT		foF2 no dawn occ.		foF2 dawn occ.		foE	
	Sep.	Sph.	Sep.	Sph.	Sep.	Sph.	Sep.	Sph.	Sep.	Sph.
# comparisons	30	30	114	114	90	90	24	24	16	16
mean (%)	-0.9	-3.8	1.6	0.3	0.0	-1.8	7.8	8.3	-4.2	-14.8
rms (%)	11.0	22.2	8.8	14.1	6.9	11.2	13.6	21.5	15.0	21.0

Table 2. Fractional differences between ionosonde measured frequencies and occultation derived frequencies. In each column the first subcolumn corresponds to the separability hypothesis and the second subcolumn to the spherical symmetry one (extracted from Hernández-Pajares et al. 2000).

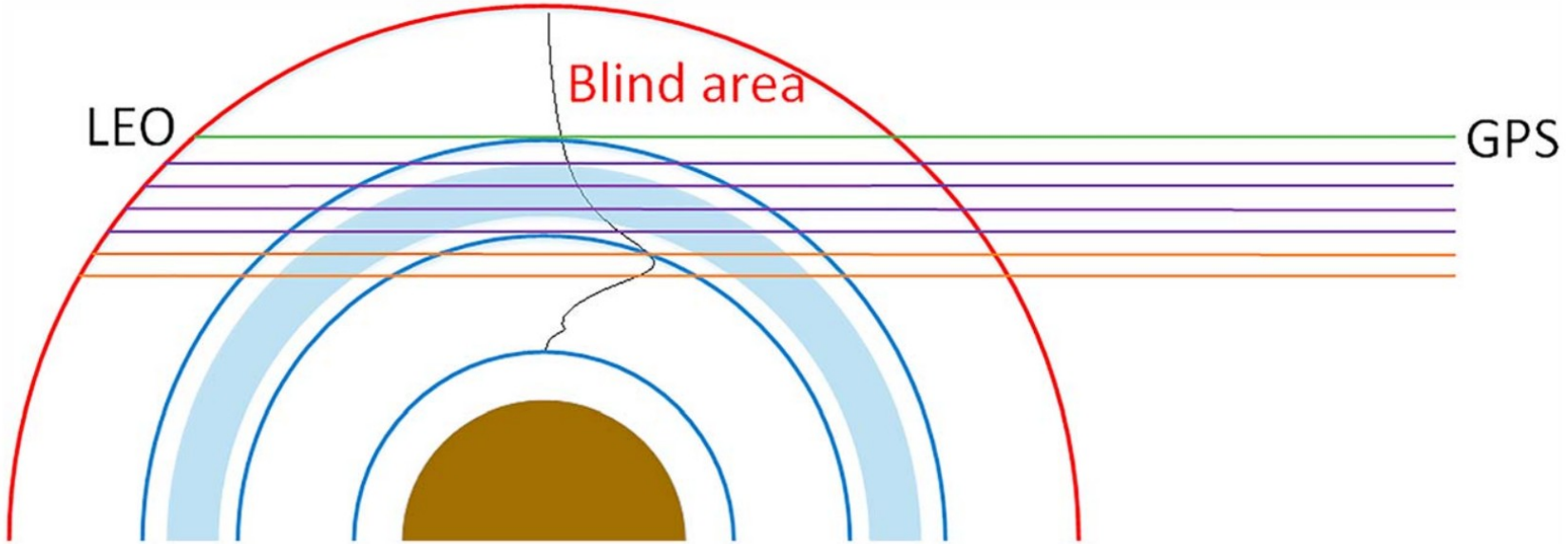

Figure 3a. Layout representing the scenario of the truncated GNSS ionospheric radio-occultations (extracted from Lyu et al. 2019).

Main equation of voxel-based GNSS data driven ionospheric electron content tomography

The underlying tomographic problem, of electron density estimation from measurements of its line-of-sight integral (the slant total electron content) measurements, can be expressed in general by the following equation:

$$L_{GF,j} \equiv L_1 - L_2 = I + B_{GF,j} = \alpha \cdot S + B_{GF,j} \simeq \alpha \cdot \sum_j N_{e,j} \cdot l_j + B_{GF,j} \qquad (1)$$

where $\alpha = 40.3 \left(\frac{1}{f_2^2} - \frac{1}{f_1^2} \right)$ in International System of Units (IS) ($\alpha \simeq 0.105$ m/TECU for L_1 and L_2 GPS frequencies, see, for example, [32]), S represents the Slant Total Electron Content (STEC), the index j runs over the number of illuminated voxels and l_j is the segment of the straight line between satellite and receiver that pierces the jth voxel. N_e is the ionospheric electron density and $B_{GF,j}$ represents the corresponding carrier phase ambiguity, both solved as an approximate random walk and random variable (constant), respectively, in a Kalman filter. The electron density random process is estimated with an update of the covariance matrix, with a process noise of $9 \cdot 10^{-8}$ (meters of $L_1 - L_2$ delay/km)^2/h. This optimal approximation has been established empirically, after 25 years of daily processing for contributing to IGS with the UPC-IonSAT global ionospheric maps (GIMs), among different tomographic experiments. The initial observation covariances are assumed to be diagonal, with an a priori standard deviation per $L_1 - L_2$ observation equation of 0.05 m.

Main equation of voxel-based GNSS data driven ionospheric electron content tomography

(1) requires only, as “sanity check”, the detection of cycle-slips of the Doppler integrated phase combinations $L_{GF,j}$.

But this problem can be understood, academically, as the estimation of matrix *A* (in general the tensor formed by the voxel electron density values), from the sums of the values of their columns or / and its rows or/and slant directions (total electron content once the lengths are taken in a simplistic way as the unity).

A very simple (2D) but directly related academic problem is exemplified in the next 2x3 matrix A, representing a low-resolution electron density distribution in a 2D vertical slice of the ionosphere (each row is associated to horizontally distributed voxels and each column with vertically distributed ones):

$$A = \begin{pmatrix} a & b & c \\ d & e & f \end{pmatrix}$$

$$A = \begin{pmatrix} a & b & c \\ d & e & f \end{pmatrix}$$

Then, the most vertical ground-based GNSS measurements of the integrated electron density, the vertical total electron content (VTEC), would correspond with the additions for each column: the three observations {V1=a+d, V2=b+e, V3=c+f}.

It is clear that the three “measurements” {V1,V2,V2}, and associated linear equations, are not enough to determine the overall electron density values, the six unknowns {a,b,c,d,e,f}, but obviously enough to estimate the VTEC, as it is shown in Figure 1c (e.g. see details in Orús et al. 2005, Hernández-Pajares et al. 2009, Roma-Dollase et al. 2018)

This is also the case when we consider separately the available GNSS radio-occultations TEC measurements in A, the additions for each row {H1=a+b+c, H2=d+e+f}.

$$A = \begin{pmatrix} a & b & c \\ d & e & f \end{pmatrix}$$

The measurement of {H1,H2} don't allow to estimate the 6 electron density values (components of the matrix A) unless some additional hypotheses are taken:

(1) the most frequent is the spherical symmetry hypothesis, the electron density profile don't change when we move horizontally: a=b=c & d=e=f => a=H1/3 & d=H2/3 is applied, or

(2) the hypothesis -significantly more general- of the electron density separability: the shape functions, formed by the electron density values normalized by the VTEC, is considered to fulfill spherical symmetry within each radio-occultation region (Hernández-Pajares et al. 2000). Then:

{a/V1=b/V2=c/V3=A & d/V1=e/V2=f/V3=D} => {H1=A*V1+A*V2+A*V3=A(V1+V2+V3) & H2=...=D(V1+V2+V3)} => => {A=H1/(V1+V2+V3) & D=H2/(V1+V2+V3)}

and, under the hypothesis assumption, the full electron density values can then be obtained as {a=A*V1, …, f=D*V3}, with a significant improvement, compared for instance with independent ionosonde measurements (see for example Table 2).

Validation vs ionosonde data & new challenging GNSS radio-occultation scenarios

	Internal comparisons		foF2 all LT		foF2 no dawn occ.		foF2 dawn occ.		foE	
	Sep.	Sph.	Sep.	Sph.	Sep.	Sph.	Sep.	Sph.	Sep.	Sph.
# comparisons	30	30	114	114	90	90	24	24	16	16
mean (%)	-0.9	-3.8	1.6	0.3	0.0	-1.8	7.8	8.3	-4.2	-14.8
rms (%)	11.0	22.2	8.8	14.1	6.9	11.2	13.6	21.5	15.0	21.0

Table 2. Fractional differences between ionosonde measured frequencies and occultation derived frequencies. In each column the first subcolumn corresponds to the separability hypothesis and the second subcolumn to the spherical symmetry one (extracted from Hernández-Pajares et al. 2000).

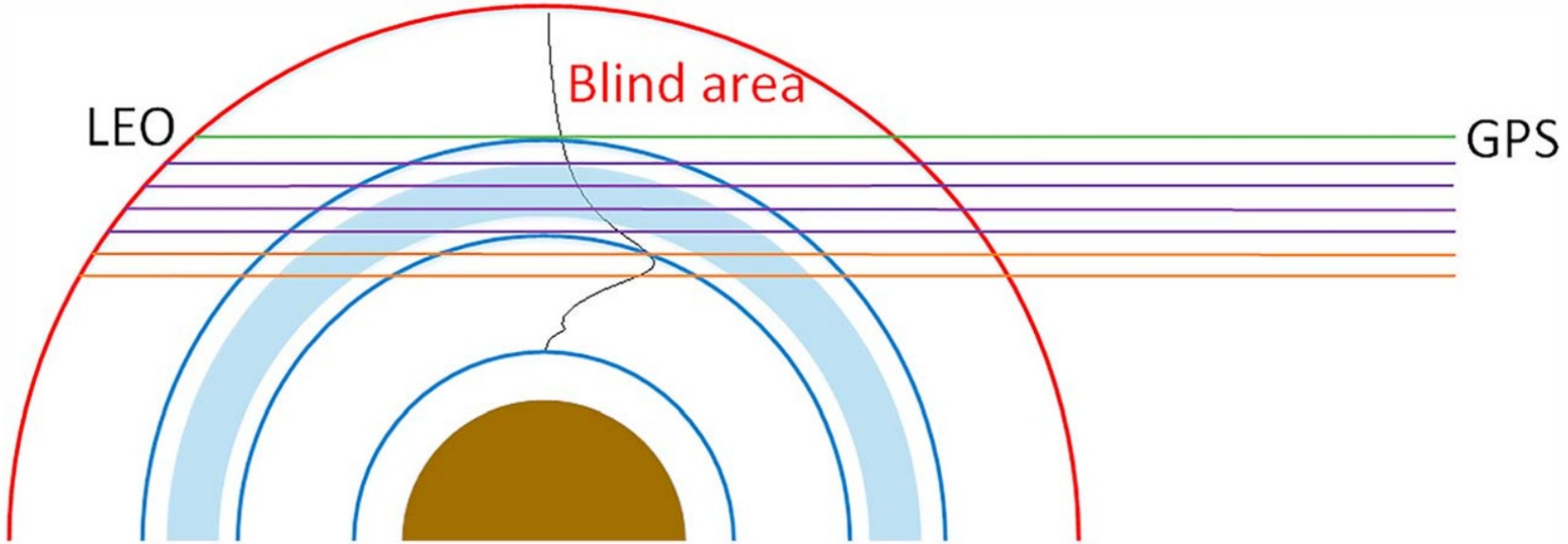

Figure 3a. Layout representing the scenario of the truncated GNSS ionospheric radio-occultations (extracted from Lyu et al. 2019).

A new challenging scenario: the truncated GNSS radio-occultations

And in new missions, like the EPS-SG EUMETSAT mission, new challenges appear: the GNSS radio-occultations are truncated at the top part, from about 500km up (prioritizing the measurements at the lower range of heights for tropospheric estimation).

In such a case a realistic and simple first-principle based assumption is very helpful: the linearly increasing topside scale height of the Chapman model, associated with the increase in the temperature, i.e. linear vary-chapman model (see e.g. Olivares-Pulido et al. 2016).

This provides the “topside skeleton” to accurately invert the most part of the radio-occultations without measurements above around 500 km (i.e. significantly below the height of many LEO-based GNSS receivers, at around 800 km height, see figures 3a, 3b & 3c below, Hernández-Pajares et al. 2017, dos Santos Prol et al. 2018B, 2019, Lyu et al. 2019 & Olivares-Pulido et al. 2023).

Truncated ionospheric GNSS radio-occultations: Example and validation

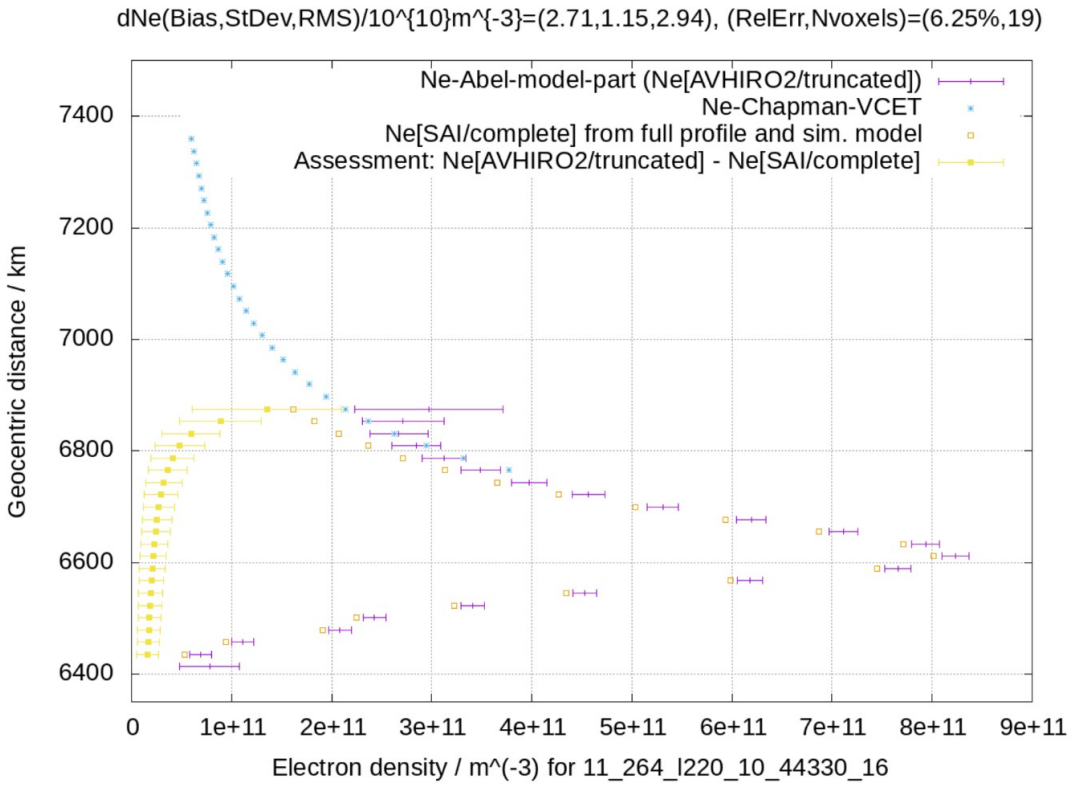

Figure 3b. Layout representing the scenario of the truncated GNSS ionospheric radio-occultations, above 500 km height, compared with the inversion of the full radio-occultation data, corresponding to COSMIC constellation data during day 264 of year 2011 (extracted from Lyu et al. 2019).

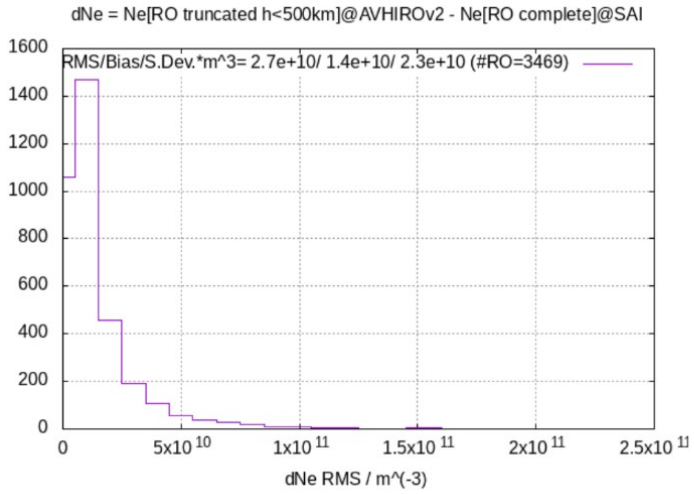

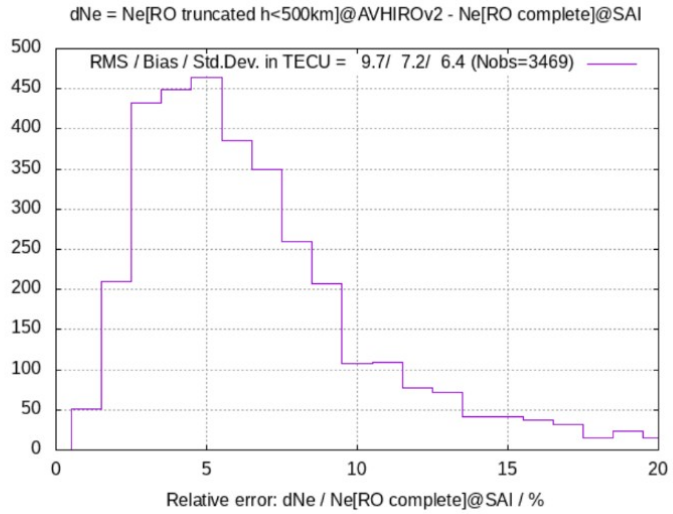

Figure 3c. Left: Histogram of the absolute ionospheric electron density RMS per RO for the linear Vary Chapman model AVHIROv2. Right: Histogram of the relative ionospheric electron density error per RO for AVHIROv2 regarding the same spherical Abel inversion model (SAI) but with the complete RO dataset (extracted from Olivares-Pulido et al. 2023).

4D tomography from measurements of ground- and radio-occultation based GNSS

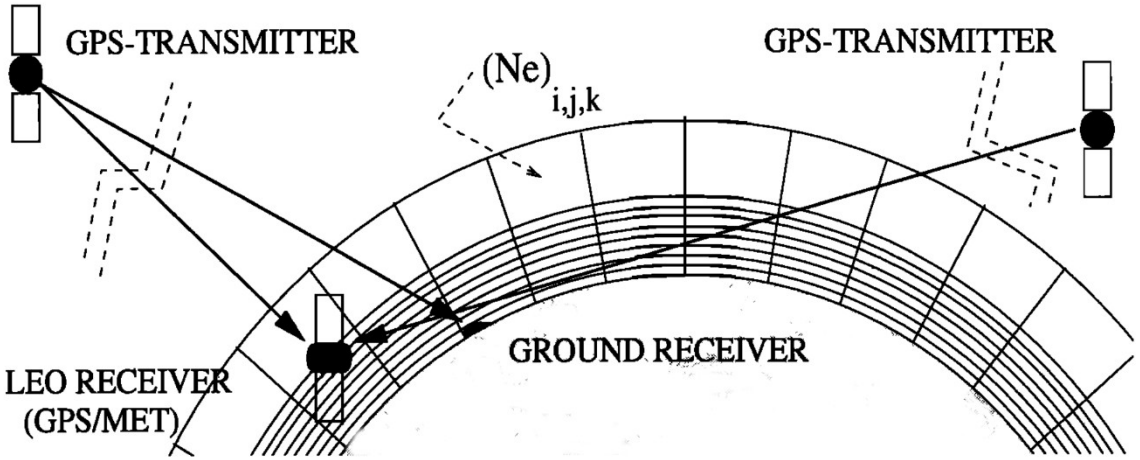

Figure 4a: Layout summarizing the combination of ground-based standard and LEO-based radio-occultation GNSS measurements for a given pair of observations line-of-sights (extracted from Hernández-Pajares et al. 1998).

A way to estimate directly the electron density of the full set of voxels (without the spherical symmetry or separability hypothesis then), represented in a very simple case by the matrix A, would be to combine the {H1, H2} (radio-occultation measurements, gathered from below the local LEO horizon) and {V1, V2, V3} measurements (ground-based one), but also slant observations from the ground GNSS receivers {S1=a+e , S2=b+f, S3=b+d, S4=c+e}.

$$A = \begin{pmatrix} a & b & c \\ d & e & f \end{pmatrix}$$

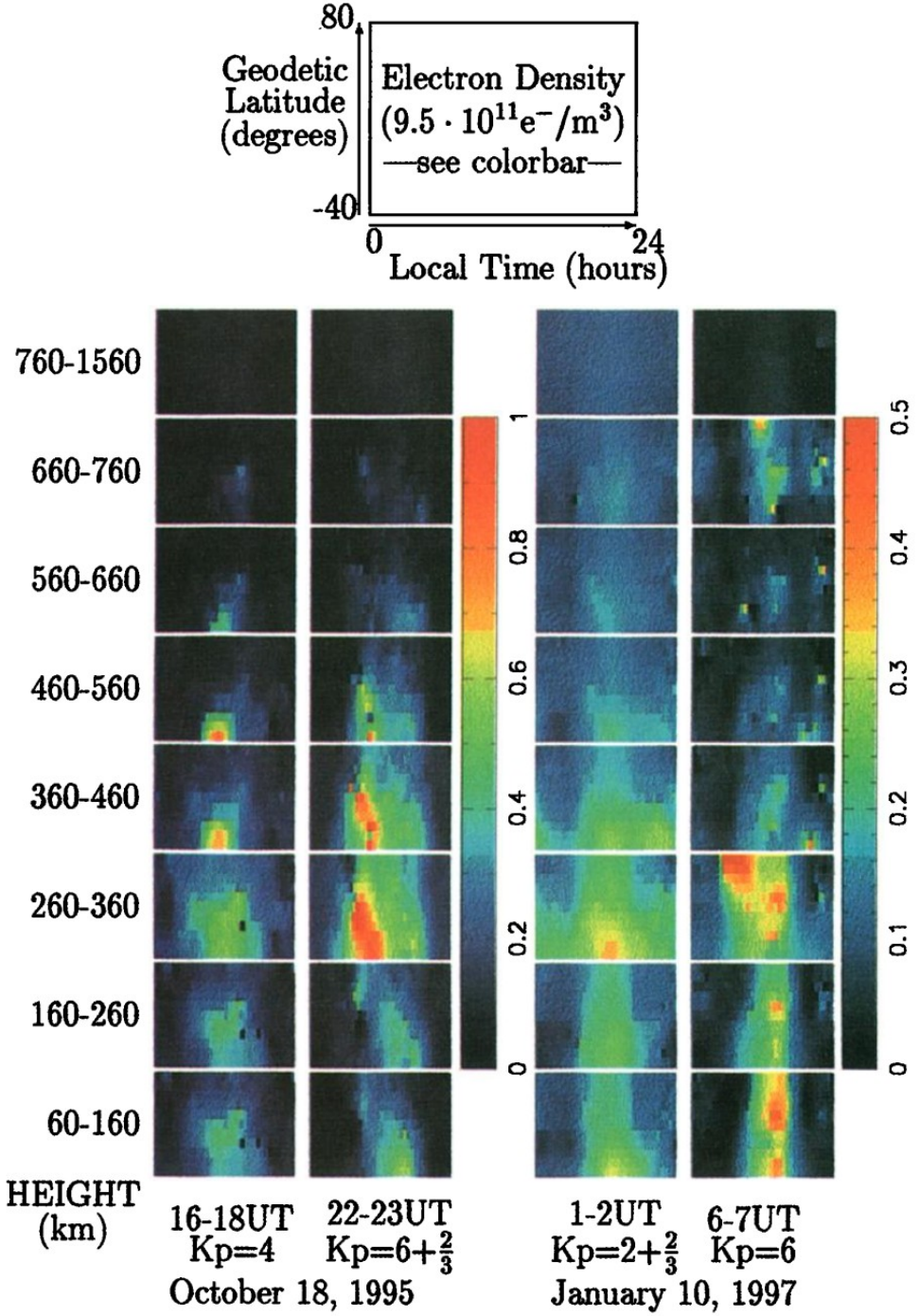

As result of this approach: First GPS tomographic imaging for studying ionospheric storms

This approach (see layout at Figure 4a) was applied in a realistic scenario in Hernández-Pajares et al. 1998, by combining measurements gathered from the IGS global network of ground-based receiver and radio-occultation measurements from GPS/MET LEO GPS receiver.

Some of the main results can be seen in Figure 4b. And, following the review paper Bust & Mitchell 2008, the above-mentioned work “initiated the use of GPS tomography for studying ionospheric storms”.

Figure 4b. Sample of the results obtained for the ionospheric storms of October 18-19, 1995 (color scale from 0 to 1012 e/m3) and January 9-10, 1997 (color scale from 0 to 1012 e/m3), combining ground-based and LEO(GPS/MET)-based radio-occultation dual-frequency GPS carrier phase measurements (extracted from Hernández-Pajares et al. 1998).

Further improvement of the tomography resolution

A still better geometry for a direct full resolution of the voxels' electron density (I.e. A matrix) consists on adding to the system of equations expressing the radio-occultations {H1, H2}, the ground-based {V1,V2,V3} and the full slant observations {S1,S2,S3,S4} in terms of the A (electron density) terms, two additional kind of observations:

(1) The topside slant observations provided by LEO Precise Orbit Determination (POD) GNSS receiver above its local horizon {sT1=a, sT2=b,sT3=c}. They allow by themselves to perform an accurate two-shell topside tomography above the LEOs (see external assessment of the derived Differential Code Biases values from this singular tomography in Figure 5a, and details in Hernández-Pajares et al. 2023).

(2) The bottom slant observations {sB1=d, sB2=e, sB3=f}, provided for instance by the Doppler observations from the DORIS transmitters at the ground, and gathered from the corresponding receivers at the corresponding LEOs, such as Cryosat-2 (CS2), JASON-3 (JA3), HY-2A (H2A), Sentinel-3 (S3A) and Saral (SRL), using as well vessel-based measurements overseas with poor coverage (see figures 5b and 5c, and details in Hernández-Pajares et al. 2020).

$$A = \begin{pmatrix} a & b & c \\ d & e & f \end{pmatrix}$$

Validation of the topside POD GNSS only based ionospheric tomography

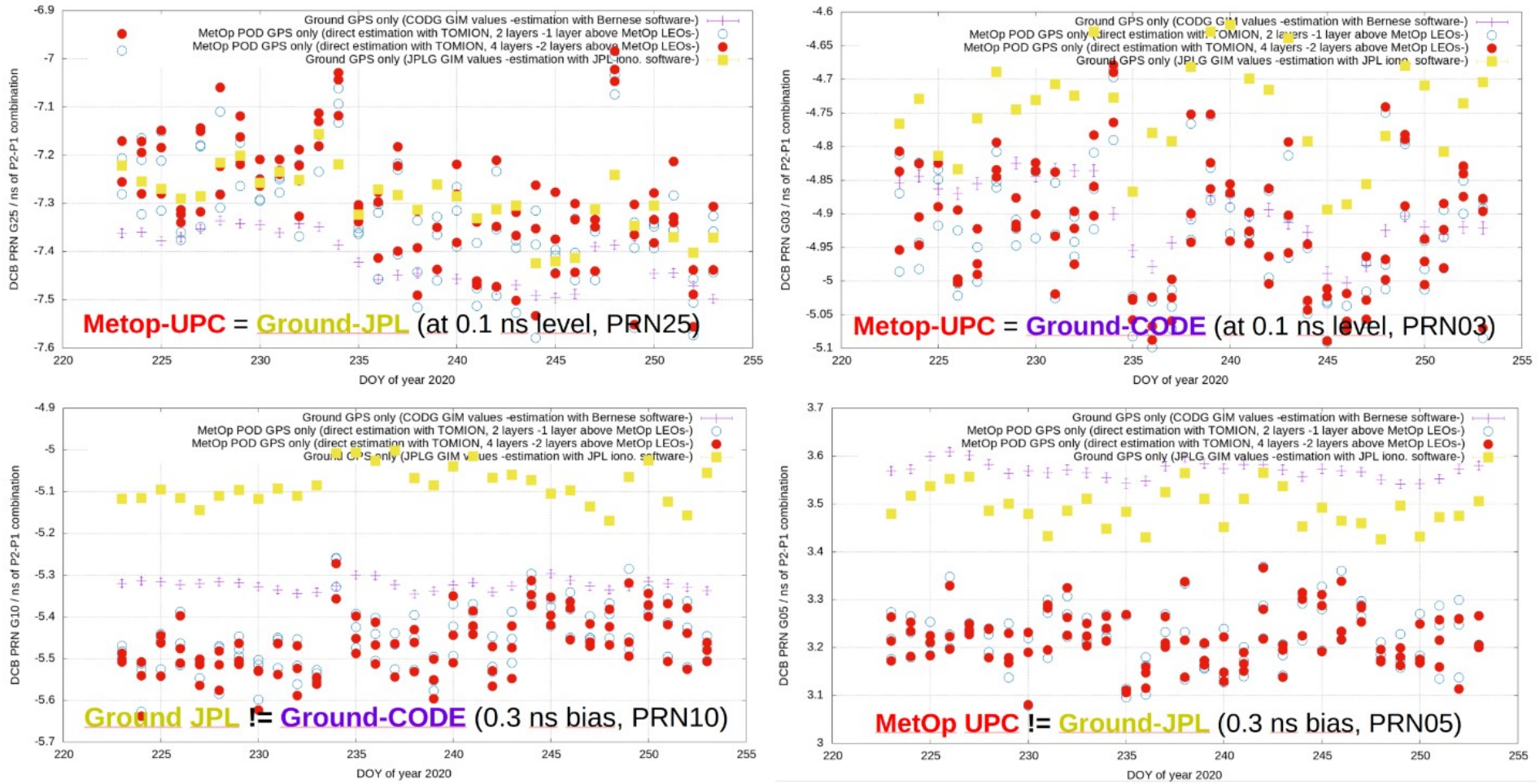

Figure 5a. Four typical examples of comparison of GPS transmitter DCBs obtained by TOMION runs based on MetOp LEO data only (2 and 4 layers, i.e., 1 and 2 layers above) vs. ground-based values from IGS centers (CODE and JPL): PRN25 (top − left), PRN03 (top − right), PRN10 (bottom − left) and PRN05 (bottom − right, extracted from Hernández-Pajares et al. 2023).

The voxel-based ionospheric tomography allows to easily allocate and exploit different kind of Space Geodesy measurements

System	Type			Height		# obs.
	Carriers	Receiver	Transmitter	Receiver	Transmitter	/1000
GPS	L1, L2	Vessel	MEOs	Sea-level	20,200 km	946
GPS	L1, L2	LEO-Sent3	MEOs	800 km	20,200 km	305
GPS	L1, L2	LEO-SWA	MEOs	460 km	20,200 km	317
GPS	L1, L2	LEO-SWB	MEOs	530 km	20,200 km	320
GPS	L1, L2	LEO-SWC	MEOs	460 km	20,200 km	317
DORIS	S1, U2	LEO-CS2	Stations	725 km	Ground	31
DORIS	S1, U2	LEO-H2A	Stations	975 km	Ground	35
DORIS	S1, U2	LEO-JA3	Stations	1345 km	Ground	51
DORIS	S1, U2	LEO-S3A	Stations	800 km	Ground	34
DORIS	S1, U2	LEO-SRL	Stations	790 km	Ground	33
Galileo	E1, E5a	Stations	MEOs	Ground	23,230 km	2825
GPS	L1, L2	Stations	MEOs	Ground	20,200 km	12,368

Table 3. Main characteristics of the different type of measurements combined under TOMION, including LEO GPS receivers Sentinel-3 (Sent3), SWARM-A (SWA), -B (SWB) and -C (SWC), and LEO DORIS receivers Cryosat-2 (CS2), HY-2A (H2A), JASON-3 (JA3), Sentinel-3 (S3A) and Saral (SRL). The types of data are S1 (2036.25 MHz) and U2 (401.25 MHz) for DORIS, E1 (1575.42 MHz) and E5a (1176.45 MHz) for Galileo, and L1 (1575.42 MHz) and L2 (1227.60) for GPS, with a typical measurement precision better than 0.1 TECUs. The corresponding number of processed observations, in thousands, are also indicated in the last column (extracted from Hernández-Pajares et al. 2020).

Figure 5b. F.S. Maria D. Merian, research vessel operated by the University of Hamburg, providing the corresponding kinematic GNSS ionospheric measurements in Hernández-Pajares et al. (2020).



Estimated electron density & further applications

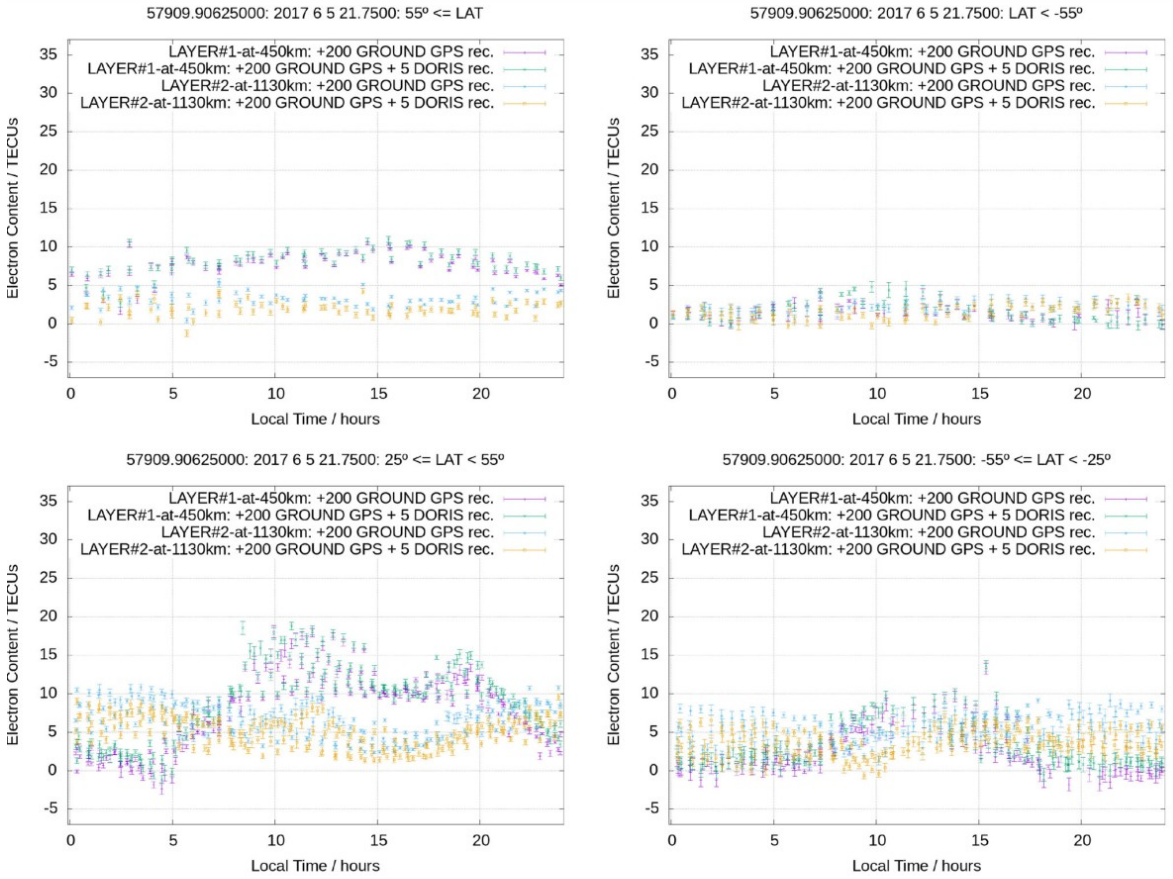

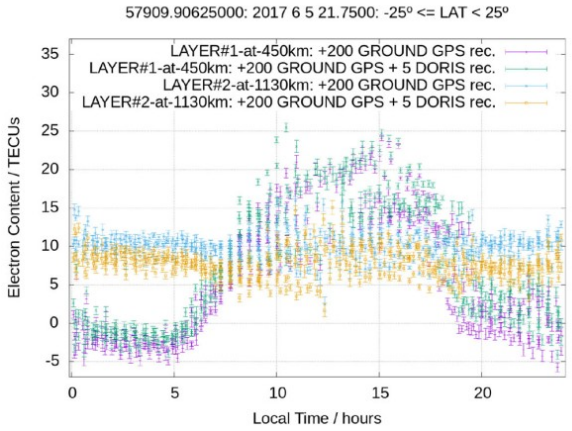

The voxel-based and external-apriori-model-free ionospheric TOMION model, is an alternative to those using a background model. Additional results are:

(1) TOMION (ground GNSS only) is able to detect vertical uplift of electron density in agreement with tsunamis (see Figure 6, and Alfonsi et al. 2024),

(2) The dual-shell TOMION model global runs improve the Faraday rotation (ionospheric 2nd order) correction induced by the Earth ionosphere electron density and by the geomagnetic field in pulsar LOFAR radio-observations (see Figure 7 & Porayko et al. 2023).

Figure 5c. Each plot represents versus local time the vertical electron content of the first layer [110–790] km by using ground GPS data only (magenta) and ground GPS and DORIS data (green), and the vertical electron content of the second layer [790–1470] km with GPS data only (blue) and ground GPS and DORIS (yellow). Each plot corresponds to GPS time of 21.75 h during June 5th, day 156 of 2017. From top to bottom and from left to right, the plots are for north high-latitudes, south high-latitudes, north mid-latitude, south mid-latitudes and low latitudes, respectively (extracted from Hernández-Pajares et al. 2020).

Recent results: Tsunami signatures & PULSAR corrections

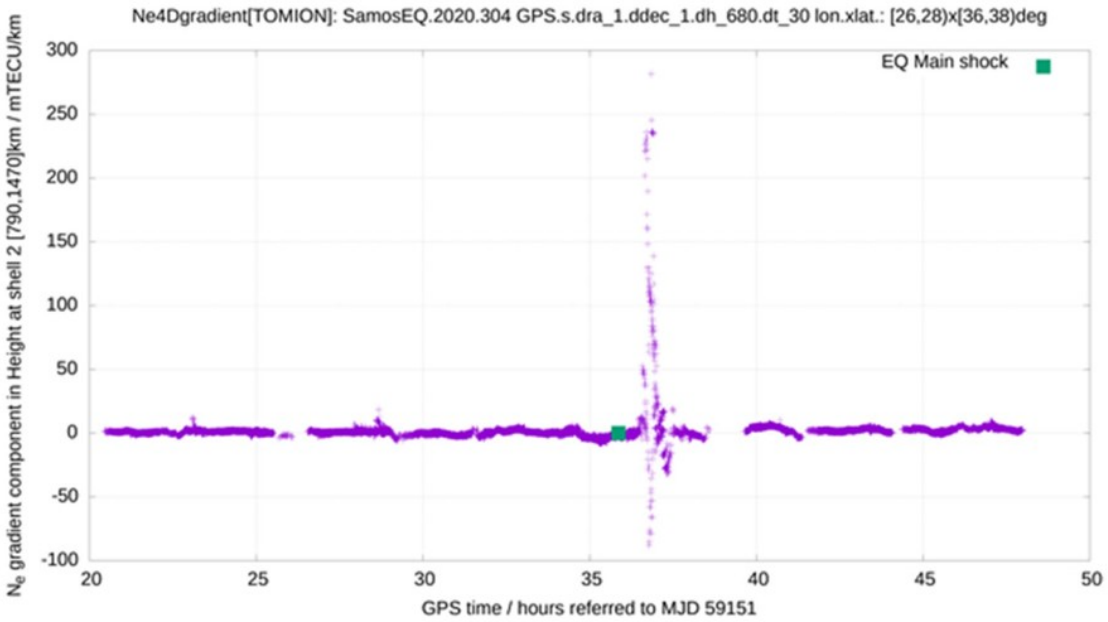

Figure 6. Vertical component of the Ne gradient estimated during October 30, 2020 with TOMION among the two-layers, with central heights at 450 km and 1130 km during the earthquake day, in the bin 26°–28°N, 36°–38° E, and using ground-based GNSS measurements only in the Eastern Mediterranean Sea.

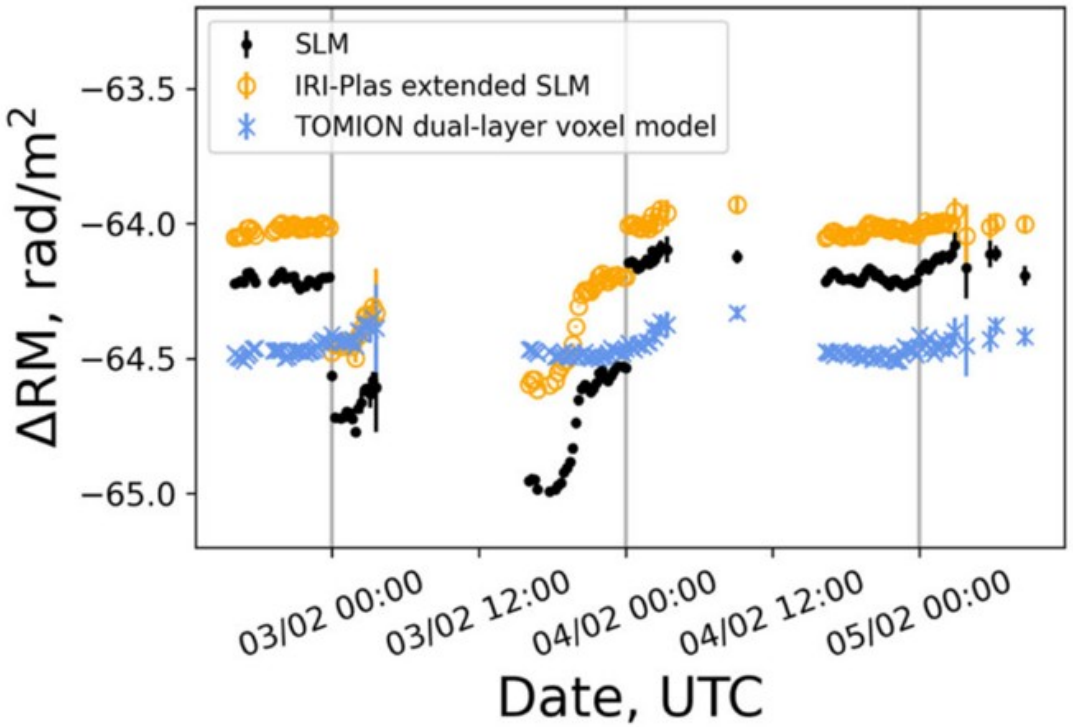

Figure 7. Corresponding Rotation Measure of the Faraday rotation (RM) residuals after the UQRG GIM Single Layer Model (SLM, black), IRI-Plas extended SLM (orange) and TOMION dual-layer voxel model (blue) are subtracted from the observed values. For demonstrative purposes, additional shifts of +0.3 rad m−2 and −0.3 rad m−2 were introduced for the latter two models. Mean value of difference of RM corresponds to the contribution of the interstellar medium, ISM (see more details in Porayko et al. 2023).

Additional types of spaceborne measurements

Among the above discussed and referenced direct electron content space-borne measurements provided by the mentioned missions with GNSS and DORIS receivers (and new ones like COSMIC-2 and Fengyun), additional types of ionospheric measurements are also provided by other missions, like:

(1) The LEO in-situ Langmuir probe electron density measurements, by missions like Swarm (see application for validating ionospheric tsunami signatures from POD GNSS measurements above the LEO in Yang et al. 2022).

(2) The UV observations, provided by the GUVI instrument on board TIMED mission (it allows to estimate the relative concentration [O/N2] very helpful to better understand the evolution of ionospheric storm phases, see for instance Figure 7 in Smirnov et al. 2026).

(3) The neutral thermospheric temperature scans provided by GOLD, also useful to understand the development the ionospheric storms (see for instance Figure 8 in the above-mentioned paper).

References

• Hervás, M., Bergadà, P., & Alsina-Pagès, R. M. (2020). Ionospheric Narrowband and Wideband HF Soundings for Communications Purposes: A Review. Sensors, 20(9), 2486. https://doi.org/10.3390/s20092486

• Wang, J., Shi, Y., Yang, C., & Feng, F. (2022). A review and prospects of operational frequency selecting techniques for HF radio communication. Advances in Space Research, 69(8), 2989–2999. https://doi.org/10.1016/j.asr.2022.01.026

• Galkin, I.A. (2021), Ionospheric Imaging with Ionosondes: Historical Perspective and Prospective Insight, in 100 Years of the International Union of Radio Science, eds. P. Wilkinson, P.S. Cannon, and W.R. Stone. URSI Press, Gent, Belgium.

• Global Ionosphere Radio Observatory, https://giro.uml.edu

• Alfonsi, L., Cesaroni, C., Hernandez-Pajares, M., Astafyeva, E., Bufféral, S., Elias, P., Belehaki, A., Ioanna, T., Yang, H. & Guerra, M. (2024), Ionospheric response to the 2020 Samos earthquake and tsunami. Earth, Planets and Space, 76:13, https://doi.org/10.1186/s40623-023-01940-2

• Bust, G. S., & Mitchell, C. N. (2008). History, current state, and future directions of ionospheric imaging. Reviews of Geophysics, 46(1).

• Cardellach, E.; Oliveras, S.; Rius, A.; Tomás, S.; Ao, C.; Franklin, G.; Iijima, B.; Kuang, D.; Meehan, T.; Padullés, R.; et al. (2019). Sensing heavy precipitation with GNSS polarimetric radio occultations. Geophys. Res. Lett., 46, 1024–1031.

• dos Santos Prol, F., de Oliveira Camargo, P., Hernández-Pajares, M. & Honorato Muella, M.T.d.A. (2018). A New Method for Ionospheric Tomography and Its Assessment by Ionosonde Electron Density, GPS TEC, and Single-Frequency PPP. IEEE TRANSACTIONS ON GEOSCIENCE AND REMOTE SENSING, DOI 10.1109/TGRS.2018.2874974.

References

• dos Santos Prol, F. D. S., Hernández-Pajares, M., Camargo, P. D. O., & Muella, M. T. D. A. H. (2018b). Spatial and temporal features of the topside ionospheric electron density by a new model based on GPS radio occultation data. Journal of Geophysical Research: Space Physics, 123(3), 2104-2115.

• dos Santos Prol, F., Themens, D. R., Hernández-Pajares, M., de Oliveira Camargo, P., & de Assis Honorato Muella, M. T. (2019). Linear Vary-Chap topside electron density model with topside sounder and radio-occultation data. Surveys in Geophysics, 40(2), 277-293.

• Hernández-Pajares, M., Juan, J. M., Sanz, J., & Solé, J. G. (1998). Global observation of the ionospheric electronic response to solar events using ground and LEO GPS data. Journal of Geophysical Research: Space Physics, 103(A9), 20789-20796.

• Hernández-Pajares, M., Juan, J. M., & Sanz, J. (2000). Improving the Abel inversion by adding ground GPS data to LEO radio occultations in ionospheric sounding. Geophysical research letters, 27(16), 2473-2476.

• Hernández-Pajares, M., Juan, J. M., Sanz, J., Orus, R., Garcia-Rigo, A., Feltens, J., ... & Krankowski, A. (2009). The IGS VTEC maps: a reliable source of ionospheric information since 1998. Journal of Geodesy, 83(3), 263-275.

• Hernández-Pajares, M., Garcia-Fernàndez, M., Rius, A., Notarpietro, R., von Engeln, A., Olivares-Pulido, G., ... & García-Rigo, A. (2017). Electron density extrapolation above F2 peak by the linear Vary-Chap model supporting new Global Navigation Satellite Systems-LEO occultation missions. Journal of Geophysical Research: Space Physics, 122(8), 9003-9014.

• Hernández-Pajares, M., Lyu, H., Garcia-Fernandez, M., & Orus-Perez, R. (2020). A new way of improving global ionospheric maps by ionospheric tomography: Consistent combination of multi-GNSS and multi-space geodetic dual-frequency measurements gathered from vessel-, LEO-and ground-based receivers. Journal of Geodesy, 94(8), 73.

References

• Hernández-Pajares, M., Olivares-Pulido, G., Hoque, M. M., Prol, F. S., Yuan, L., Notarpietro, R., & Graffigna, V. (2023). Topside ionospheric tomography exclusively based on LEO POD GPS carrier phases: Application to autonomous LEO DCB estimation. Remote Sensing, 15(2), 390.

• Lyu, H., Hernández-Pajares, M., Monte-Moreno, E., & Cardellach, E. (2019). Electron density retrieval from truncated radio occultation GNSS data. Journal of Geophysical Research: Space Physics, 124(6), 4842-4851.

• Mao, T.; Sun, L.; Yang, G.; Yue, X.; Yu, T.; Huang, C.; Zeng, Z.; Wang, Y.; Wang, J. (2016). First ionospheric radio-occultation measurements from GNSS occultation sounder on the Chinese Feng-Yun 3C satellite. IEEE Trans. Geosci. Remote Sens., 54, 5044–5053.

• Olivares-Pulido, G., Hernández-Pajares, M., Aragón-Àngel, A., & Garcia-Rigo, A. (2016). A linear scale height Chapman model supported by GNSS occultation measurements. Journal of Geophysical Research: Space Physics, 121(8), 7932-7940.

• Olivares-Pulido, G., Hernández-Pajares, M., Monte-Moreno, E., Lyu, H., Graffigna, V., Cardellach, E., ... & Garcia-Fernandez, M. (2023). Real-time tomographic inversion of truncated ionospheric GNSS radio occultations. Remote Sensing, 15(12), 3176.

• Orús, R., Hernández-Pajares, M., Juan, J. M., & Sanz, J. (2005). Improvement of global ionospheric VTEC maps by using kriging interpolation technique. Journal of atmospheric and solar-terrestrial physics, 67(16), 1598-1609.

References

• Porayko, N.K., Mevius, M., Hernández-Pajares, M., Tiburzi, C., Olivares-Pulido, G., Liu, Q., Verbiest, P.W., Künsemöller, J., Ambalappat Krishnakumar, M., Bak Nielsen, A.-S., Brüggen, M., Graffigna, V., Dettmar, R.-J., Kramer, M., Osłowski, S., Schwarz, D.J., Shaifullah, G.M., & Wucknitz, O. (2023). Validation of global ionospheric models using long-term observations of pulsar Faraday rotation with the LOFAR radio telescope. Journal of Geodesy 97-116, https://doi.org/10.1007/s00190-023-01806-1

• Roma-Dollase, D., Hernández-Pajares, M., Krankowski, A., Kotulak, K., Ghoddousi-Fard, R., Yuan, Y., ... & Gómez-Cama, J. M. (2018). Consistency of seven different GNSS global ionospheric mapping techniques during one solar cycle. Journal of Geodesy, 92(6), 691-706.

• Yang, H., Hernández-Pajares, M., Jarmołowski, W., Wielgosz, P., Vadas, S. L., Colombo, O. L., ... & Haagmans, R. (2022). Systematic detection of anomalous ionospheric perturbations above LEOs from GNSS POD data including possible tsunami signatures. IEEE Transactions on Geoscience and Remote Sensing, 60, 1-23.